Semi-empirical approach to the simulation of molecule-surface reaction dynamcis

Migliorini, D.

Chapter 5

Methane on a Stepped Surface: Dynamical Insights on the Dissociation of CHD_3 on Pt(111) and Pt(211)

This Chapter is based on:

D. Migliorini, H. Chadwick, and G. J. Kroes *J. Chem. Phys.*, 149, 094701 (2018)

which is reproduced with the permission of AIP publishing.

Abstract

The simulation of the dissociation of molecules on metal surfaces is a cornerstone for the understanding of heterogeneously catalyzed processes. However, due to high computational demand, the accurate dynamical simulation of the dissociative chemisorption of polyatomic molecules has been limited mostly to flat low-index metal surfaces. The study of surfaces that feature "defected" sites, such as steps, is crucial to improve the understanding of the overall catalytic process due to the high reactivity of under-coordinated sites for this kind of reaction. In this work we have extensively analyzed more than 10000 AIMD tra-

jectories where a CHD_3 molecule is impinging either on the flat Pt(111) or on the stepped Pt(211) surface for different initial rovibrational states and collision energies. The results have been compared in order to get insights into the effect of the step on the dissociation of methane. We have found that, despite a large difference in the activation barrier and consequently in reactivity, the geometry of the lowest transition states is very similar on the two surfaces and this results in a similar dissociation dynamics. Furthermore, the trapping observed on the Pt(211) surface can be explained with energy transfer to parallel translational motion induced by the geometry of the slab and by a larger energy transfer to phonons for the stepped Pt(211) surface.

5.1 Introduction

The dissociative chemisorption of methane on a transition metal surface has been employed, both theoretically [1–10] and experimentally [11–14], as a model system to understand one of the most important steps in steam reforming [15], a fundamental industrial process which is currently one of the most common ways to produce molecular hydrogen. The CH bond cleavage on a Ni or Pt based catalyst is believed to be one of the rate determining steps [15] of the overall process in the high temperature regime. Due to the large complexity of molecule-surface reactions and to the necessity of treating accurately both the molecule and the metal slab, these systems have always been challenging for appropriate dynamical simulations [16–21]. The large number of degrees of freedom (DOFs) makes density functional theory (DFT) at the generalized gradient approximation (GGA) or meta-GGA level the go-to method for these systems and excludes any higher level of theory, at least for dynamical simulations [22]. Unfortunately, standard GGA and meta-GGA functionals are known for their poor accuracy in the calculation of activation barriers (E_b) [22] for molecule-surface systems; this has encouraged, in the last few decades, the pursuit of semi-empirical functionals [3, 5, 23–25] able to compute activation barriers with errors as small as 1 kcal/mol ($\approx$ 4.2 kJ/mol), so-called chemical accuracy.

One of the viable semi-empirical methods to develop an accurate density functional is a variation of the specific reaction parameter (SRP) approach originally proposed by Truhlar and coworkers [26]. In our implementation for molecules on metals this approach consists of mixing two GGA functionals through a mixing parameter so that the SRP functional is able to reproduce the experimental zero-coverage reaction probability (S_0) with chemical accuracy. This has been applied successfully to different catalytically relevant systems where a molecule dissociates on a low-index flat metal surface [3, 5, 23–25]. Recently, chemical accuracy has been achieved for CHD_3 on Ni(111) [5] using the SRP32-vdW functional obtained by mixing the RPBE [27] and the PBE [28, 29] exchange functionals (E_X^{RPBE} and E_X^{PBE}, respectively) with a mixing parameter $x = 0.32$ and using the correlation functional developed by Dion *et al.* [30, 31] ($E_C^{\text{vdW-DF}}$) that also models van der Waal interactions. The exchange correlation part of the SRP32-vdW functional ($E_{XC}^{\text{SRP32-vdW}}$) reads as:

$$E_{XC}^{\text{SRP32-vdW}} = 0.32 \cdot E_X^{RPBE} + (1 - 0.32) \cdot E_X^{PBE} + E_C^{\text{vdW-DF}}. \tag{5.1}$$

The SRP32-vdW functional has been successfully transferred from CHD_3 dissociation on Ni(111) to Pt(111) and, more importantly, it was able to achieve chemical accuracy also on the stepped Pt(211) surface, as shown in Chapter 4 and in Ref. [3]. The transferability of the SRP functional from the flat Pt(111) to the stepped Pt(211) surface suggests that an SRP functional developed for a relatively simple system, such as the flat (111) surface, can be used to obtain accurate reaction barriers on different defected sites of the same metal (see Chapter 4, Ref. [3] and references therein). The study of a stepped transition metal surface such as Pt(211) is highly relevant for heterogeneous catalysis since it is known that under-coordinated sites usually show enhanced reactivity for processes like the dissociative chemisorption of methane [32–36]. Moreover the dissociation of methane on Pt(211) has been previously used to model the overall catalytic process through microkinetic simulations [1, 2].

In this Chapter we report the analysis of 12500 *ab initio* molecular dynamics

(AIMD) trajectories of CHD_3 impinging on Pt(111) and Pt(211) in order to study and compare the dynamical features of the dissociation on the two surfaces, focusing on the differences introduced by the presence of the step. The Chapter is organized as follows: the method used to setup, propagate and analyze the trajectories is reported in Section 5.2, the results are presented and discussed in Section 5.3 and the main conclusions are summarized in Section 5.4.

5.2 Method

Most of the results discussed in this Chapter have been obtained by analyzing AIMD trajectories of CHD_3 impinging on the Pt(111) and on the Pt(211) surfaces. These simulations have been used to compute the zero-coverage reaction probability (S_0) which has been compared to molecular beam experiments to define and test the SRP32-vdW functional for said systems [3]. The computational details have been recently published [3] and therefore, they will only be summarized in this Section.

The electronic structure calculations have been performed on a DFT level using the Vienna *ab initio* simulation package (VASP) [37–40] version 5.3.5. The first Brillouin zone has been sampled with a 4x4x1 Γ-centered K-point grid and the basis set includes plane waves with kinetic energy up to 350 eV. The core electrons have been represented through projector augmented-wave (PAW) pseudopotentials [41, 42]. The Pt(111) surface has been represented using a 5 layer (3x3) supercell slab, consistent with previous work [3, 6]. The stepped Pt(211) surface has been modelled using a 4 layer (1x3) supercell. For both surfaces, the slab is separated from its first periodic replica by 13 Å of vacuum. A 0.1 eV Fermi smearing has been used to facilitate the SCF convergence. The setup used for these calculations has been extensively tested and the results of the tests are available in the Supporting Information of Ref. [3].

The AIMD trajectories have been setup in order to reproduce the molecular beam experiments performed by Beck and co-workers [3] including the surface temperature (T_s) of 500 K and 650 K for Pt(111) and Pt(211) respectively, and

modelling the initial kinetic energy and rovibrational population of the methane molecules. Note that, even though the simulations have been performed at different temperatures for the two surfaces, previous work suggests that the temperature dependence of the reactivity on Pt is small [6, 43]. Quasi-classical trajectories (i.e., classical trajectories where the vibrational zero-point energy is imparted to the molecule) have been propagated with a 0.4 fs time-step until dissociation or scattering was observed. A molecule has been considered reacted if a bond was stretched over 3.0 Å and it has been considered scattered if, after the impact, it reached a certain distance above the surface (i.e., 6.0 Å or 6.5 Å for Pt(111) and Pt(211), respectively) while the center of mass (COM) velocity was pointing away from the surface. For the reactive trajectories the time of the dissociation (t_{diss}) has been defined as the first time step at which the dissociating bond is as elongated as in the minimum energy transition state ±0.04 Å. In this work the molecules that did not reach an outcome within the first 2 ps of propagation have been considered trapped.

The transition state (TS) geometries presented have been computed using the dimer method included in the VASP transition state tools package (VTST) [44–47]. Frequency analysis calculations have been performed to confirm that all the TSs reported in this work are true 1^{st} order saddle points (i.e., one and only one imaginary frequency is present) except where stated differently. The analysis has been carried out on 7000 trajectories for Pt(111) and on 5500 trajectories for Pt(211) for an initial average incident energy ($\langle E_i \rangle$) ranging between 60.7 and 120.1 kJ/mol for Pt(111) and between 58.2 and 107.9 kJ/mol for Pt(211). Several dynamics-relevant features have been investigated and the results have been binned and smeared using a sum of Gaussian curves such that, for a sample of N data, the final distribution $\mathcal{F}(\alpha)$ of the observable α is represented as:

$$\mathcal{F}(\alpha) = \sum_{i}^{Nbins} \sum_{j}^{Ndata} \frac{1}{\sqrt{2\pi\sigma_G^2}} \cdot exp\left(- \frac{(bin_0 + i \cdot binsize - data(j))^2}{2\sigma_G^2} \right), \quad (5.2)$$

where the indices i and j run over the bins and the data respectively, bin_0 is the first value of α considered for the binning procedure and σ_G is the standard

deviation of the Gaussian used (i.e., the broadening). The final distribution is the sum of Gaussians centered on the data values for each element of the dataset. Since we are comparing datasets of different sizes the area of the final distributions is always normalized to 1. In this Chapter the distributions reported in the same plot always have the same broadening and all the distribution parameters are reported in the Supplementary Material (SM) of Ref. [48].

Using a broadening can improve the quality and the readability of the results but can cause small tails at the edge of the distribution that might assume unphysical values. However this does not affect the interpretation of the results. In order to calculate the distributions all the available trajectories have been used. This means that the distribution takes into account results for different CHD_3 vibrational states and average collision energies (see Ref. [3]) unless explicitly stated. For some of the observables α, the average value is reported together with the standard deviation σ and standard error σ_M:

$$\sigma = \sqrt{\frac{\sum_{i=1}^{N}(\alpha_i - \langle\alpha\rangle)^2}{N-1}}, \tag{5.3}$$

$$\sigma_M = \frac{\sigma}{\sqrt{N}}. \tag{5.4}$$

Here, N is the sample size and $\langle\alpha\rangle$ is the sample average.

5.3 Results and Discussion

Platinum is an fcc metal and its (111) surface shows the well-known hexagonal lattice structure. The Pt(211) surface is composed of 3 atom wide (111)-like terraces and (100)-like steps. In order to analyze the dynamics on the Pt(211) surface three non-equivalent sites have been defined: edge (on the step edge), middle (the row of atoms in the middle of the terrace) and bottom (the row of atoms on the low end of the step). Moreover some of the analysis is referenced to facets instead of sites considering the step (i.e., the (100) facet) and the terrace (i.e., the (111) facet). The side and top views of the surfaces are shown in Figure

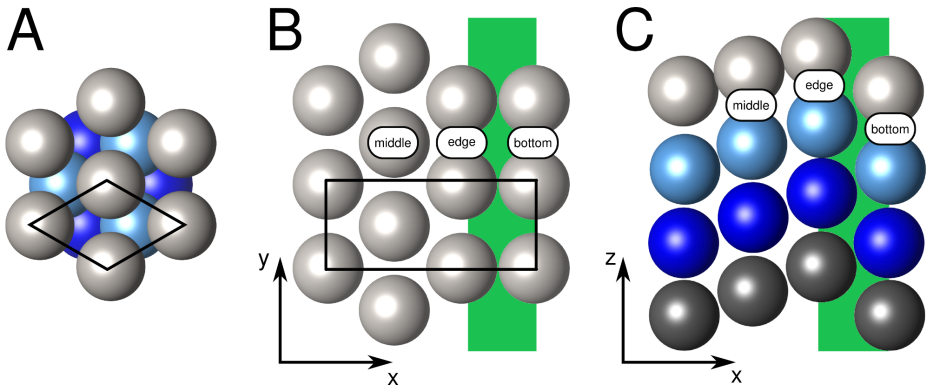

Figure 5.1: (A) top view of the Pt(111) surface. (B) top view of the first layer of the Pt(211) surface. (C) side view of the Pt(211) surface. For both the surfaces, the atoms are reported in their equilibrium position. The unit cell is marked in black and different layers are reported in different colors. For the Pt(211) surface, the three rows of atoms in the unit cell are called edge, middle, and bottom according to their position: edge is on top of the step edge, middle is in the middle of the terrace, and bottom is on the low side of the step. The (100) step is shaded in green while the remainder of the surface is the (111) terrace.

5.1 where the atoms are reported in their equilibrium positions and the step facet is highlighted in green for the Pt(211) surface. The impact (reaction) site is defined as the nearest site (i.e., bottom, middle or edge) in the xy plane at the closest approach (reaction) time. Molecules that hit the surface or dissociate at an x coordinate between the edge and the bottom site (green shaded area in Figure 5.1) are considered step facet events. It has been shown in previous work [3] and in Chapter 4 that the reactivity on the stepped surface happens almost completely through the dissociation on top of the step edge atom. Therefore the analysis of reacted trajectories has been carried out by looking at the different behavior of molecules impacting on the different surface sites (i.e., edge, middle and bottom atoms). For non-reactive trajectories the differences in the dynamics upon impacting on the (111)-like terrace facet or on the (100)-like step facet have also been considered.

On the Pt(211) surface trapping has been observed and the average trapping time has been estimated to be about 40 ps [3] (i.e., 43 ps), which is too short to be detected experimentally and too long to be simulated with an expensive method

like AIMD. For the previously published work [3], reported also in Chapter 4, the trapped trajectories have been propagated for 1 ps (or 2 ps in a few test cases). To ensure a fair analysis, in this work all the trapped trajectories have been propagated up to 2 ps. Out of the 69 trajectories that were considered trapped after 1 ps, 35 were scattered upon further propagation. However this does not necessarily affect the main conclusions of earlier work since a large number of trapped trajectories are still present even after 2 ps of propagation, especially at low incidence energy. This also suggests that, in order to be considered trapped (i.e., characterized by some average trapping time), the molecules need some time to equilibrate with the surface.

To understand the dynamics of the CHD_3 on the different surfaces, the number of bounces has been counted for all the trajectories, where a bounce is defined as two sign-changes of the COM velocity along the direction perpendicular to the macroscopic surface. As observed for other metal surfaces, the CHD_3 dissociative chemisorption is usually a "sudden" process: on both platinum surfaces the molecules react on the first impact and without bouncing. This is also true for almost all the scattered trajectories on Pt(111) (only 5 out of more than 6500 perform one and only one bounce) and for most of the scattered trajectories on Pt(211). On Pt(211) we observe a few trajectories bouncing either one or two times before scattering. The trapped trajectories bounce between one and four times during the propagation (see Figure 5.2).

5.3.1 Transition States

Several transition states have been located on the stepped Pt(211) surface by performing calculations using the dimer method [44–47]. All the TSs presented are real 1^{st} order saddle points as confirmed by a normal mode analysis unless stated differently. The energy (i.e. the barrier height, E_b), the length of the dissociating CH bond (r_b) and the θ, β and γ angles have been determined. θ is the angle between the dissociating bond and the surface normal (i.e., z) and β is the angle between the umbrella axis ($\vec{a}$) and the surface normal, where $\vec{a}$ is defined as the vector going from the geometric center of the (non-reacting)

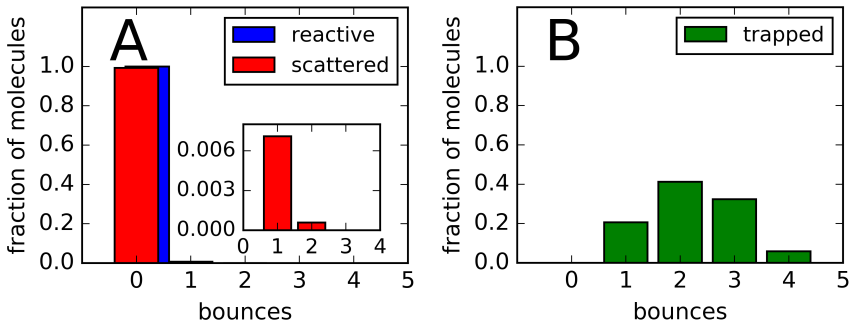

Figure 5.2: Number of bounces for the molecules impinging on the Pt(211) surface. (A) fraction of scattered and reacted trajectories in red and blue, respectively. The inset in panel A is a magnification for the few trajectories that bounce before scattering. (B) results for the trapped trajectories on Pt(211).

umbrella hydrogens to the carbon atom (Figure 5.3). γ is the angle between the dissociating CH bond and the $\vec{a}$ axis. The γ angle describes the internal geometry of the TS, while β and θ describe the geometry of the molecule with respect to the macroscopic surface normal. All the results, and the minimum energy TS for the flat Pt(111) surface, are reported in Table 5.1 including all the TS geometries (also represented in Figure 5.4) and the studied angles (also shown in Figure 5.3). The angle α (sketched in Figure 5.3 and reported in Table 5.1) describes the orientation of the dissociating bond in the xy plane for the Pt(211) surface and it will be discussed later in this Chapter.

For Pt(211), four TSs have been found on top of a step edge atom, with a different orientation of the dissociating CH bond. These have been labeled according to the positions of the carbon and of the dissociating hydrogen:
Edge2Edge-Bridge (Edge2Edge-B) dissociating parallel to the step edge (Figure 5.4B), Edge2Middle-Hollow (Edge2Mid-H) dissociating on a hollow site toward the middle row of the terrace (Figures 5.4C and 5.4D), and Edge2Bottom-Bridge (Edge2Bot-B) dissociating toward a bridge site on the (100) step site (Figure 5.4E). Note that the two TSs depicted in Figures 5.4C and 5.4D are related by a hindered rotation about the umbrella axis. Three TSs have been found on the middle terrace atom dissociating toward different bridge sites, and

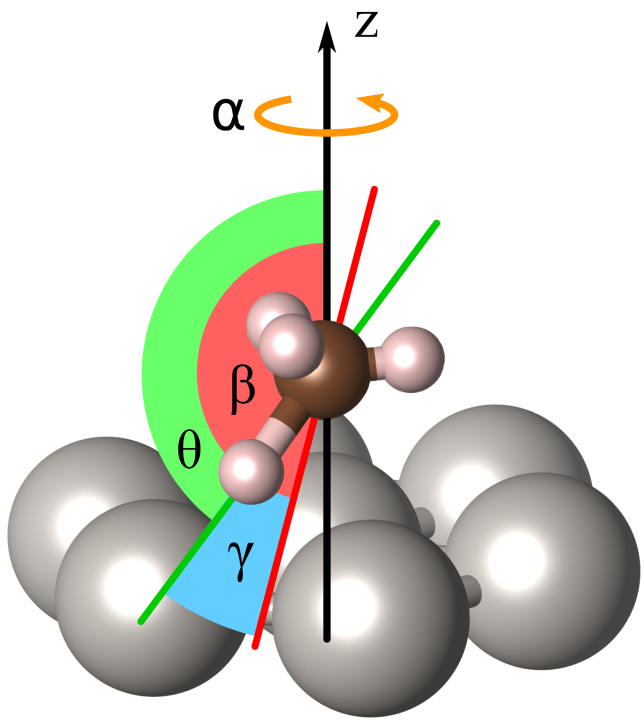

Figure 5.3: Sketch of the angles studied: θ (green shade) is the angle between the CH bond (green line) and the z axis, β (red) is the angle between the umbrella axis $\vec{a}$ (red line) and the z axis (i.e., the macroscopic surface normal), and γ (blue) is the angle between the CH bond and the umbrella axis $\vec{a}$. The angle α (orange) represents the orientation of the dissociating bond in the xy plane.

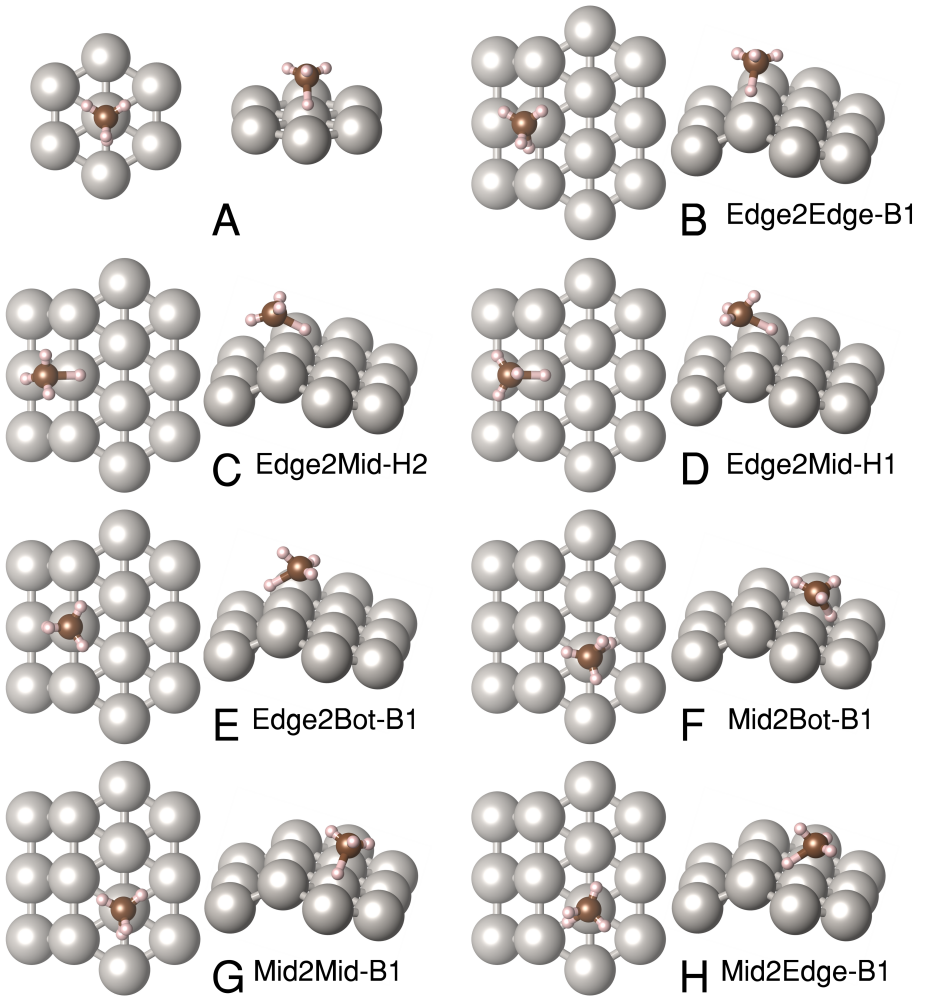

Figure 5.4: Depiction of the transition state geometries found in side and top views. TS A is the one found for Pt(111) and reported in Chapter 4 and Ref. [3]. TSs B to H have been found on Pt(211) and are also labeled with the names reported in Table 5.1.

Surface	L	Name	θ [∘]	β [∘]	γ [∘]	α [∘]	r_b [Å]	E_b [kJ/mol]
Pt(111)	A	...	133.4	168.3	34.8	...	1.55	78.6
Pt(211)	B	Edge2Edge-B1	132.9	166.0	33.1	85.0	1.53	53.9
Pt(211)	C	Edge2Mid-H2	115.6	145.6	30.0	181.3	1.60	57.1
Pt(211)	D	Edge2Mid-H1	113.7	145.9	32.2	179.4	1.62	57.7 *
Pt(211)	E	Edge2Bot-B1	122.9	156.8	33.9	0.5	1.65	65.1 *
Pt(211)	F	Mid2Bot-B1	145.8	171.8	35.0	226.3	1.55	97.9
Pt(211)	G	Mid2Mid-B1	130.2	158.5	34.9	72.1	1.57	98.0
Pt(211)	H	Mid2Edge-B1	119.0	151.7	33.4	25.3	1.56	96.4

Table 5.1: Comparison of the TSs found on the two platinum surfaces. For each, the following properties are reported: the surface on which it has been found, the label (L) as in Figure 5.4, the name of the TS, the θ, β, γ and α angles, the length of the dissociating bond (r_b) in Å, and the energy barrier (E_b) in kJ/mol. Note that if the energy barrier is followed by a star (*), the TS reported still has a second imaginary frequency (i.e., it is not a real 1^{st} order saddle-point).

they have been labeled as Middle2Bottom-Bridge (Mid2Bot-B), Middle2Middle-Bridge (Mid2Mid-B), and Middle2Edge-Bridge (Mid2Edge-B) according to which site they are dissociating toward (Figures 5.4F-5.4H, respectively). The numbers, either 1 or 2, at the end of a TS name identify the eclipsed or the staggered orientation of the umbrella relative to the dissociating CH bond, respectively. Note that the TSs depicted in Figures 5.4D and 5.4E still have a second small imaginary frequency (i.e., they are not real 1^{st} order saddle points; see Table 5.1).

There is a clear difference in the E_b between dissociation on the step edge atom and on the terrace middle atom (i.e., ≈ 39 kJ/mol on average), regardless of the molecular orientation: the TSs centered on the step edge atom have very similar energies and the same is true for the TSs centered on the terrace middle atom. The step edge site is more reactive than the flat Pt(111) surface, while terrace middle sites show barriers even larger than on the ideal flat surface (78.6 kJ/mol, Table 5.1). Despite this large range of E_b , the TSs are geometrically similar: all of them have a dissociating bond length between 1.53 and 1.65 Å and an angle γ between the dissociating bond and $\vec{a}$ between 30° and 35°. As expected

β and θ show more variability because they depend on the molecular geometry as well as on the surface orientation with respect to the reference frame (z axis). β and θ can be compared for the TS on Pt(111) and the lowest energy TS on Pt(211) (i.e., Edge2Edge-B1) and both angles have the same values within less than 2.5°.

5.3.2 Energy Transfer to Parallel Motion

In Figure 5.5, the COM lateral displacement (δ_{COM}) has been reported for all the trajectories, where δ_{COM} has been computed as the difference between the COM xy position at the initial and at the reaction step (for dissociative events) or at the step of 1^{st} closest approach (for scattered and trapped trajectories). For the flat surface, the reactive events happen in a "sudden" fashion where the molecule does not change its position in the xy plane significantly, as they show $\langle\delta_{COM}\rangle$ smaller than 0.09 Å (Figure 5.5A). The same is true for the molecules reacting on the step edge of Pt(211) (Figure 5.5B).

Scattered and trapped molecules on Pt(211) show a significantly larger $\langle\delta_{COM}\rangle$ that can go up to 0.25 Å for molecules trapped after impacting on the step facet (all the data are reported in the SM of Ref. [48]). This is due to the fact that, even though all molecules start with a COM velocity aligned with the z axis, the topology of the surface can induce energy transfer from the translational motion in the z direction to the motion along the surface (energy transfer to parallel motion). In order to study this phenomenon, the distance travelled in the xy plane has been computed (for each individual trajectory) as:

$$d_{xy} = \sum_{t=1}^{T} \sqrt{(x_t - x_{t-1})^2 + (y_t - y_{t-1})^2}, \tag{5.5}$$

$$d_{\alpha=x,y} = \sum_{t=1}^{T} \left|(\alpha_t - \alpha_{t-1})\right|, \tag{5.6}$$

Here, d_{xy} is the distance travelled in the xy plane, d_α is the distance travelled in the α direction (i.e., $\alpha = x, y$), and t is the time step. T is the total number

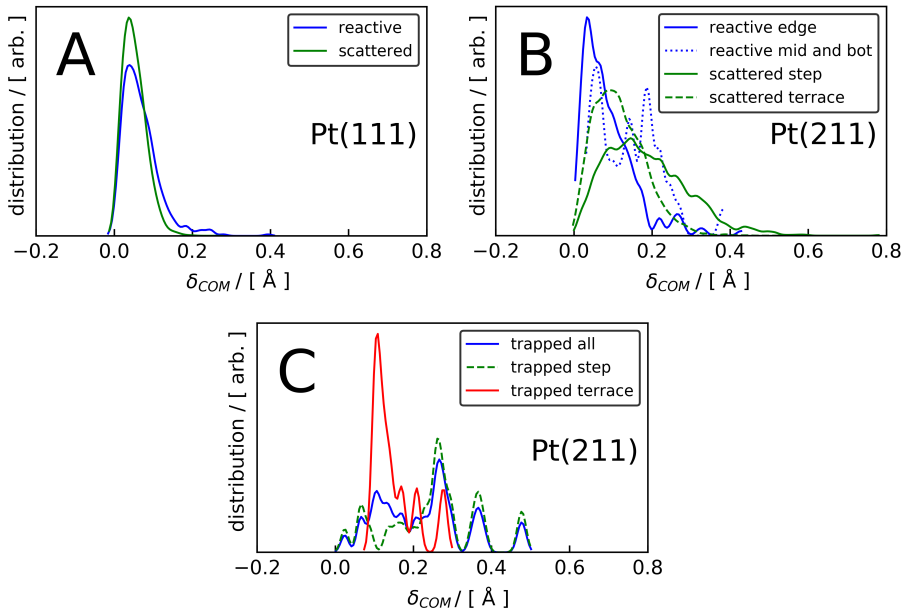

Figure 5.5: (A) δ_{COM} computed for the reactive (blue) and scattered (green) trajectories on Pt(111). (B) δ_{COM} computed for the reactive (blue) and scattered (green) trajectories on Pt(211), the solid lines describe step edge atom reaction and step facet scattering, the dotted line describes bottom and middle atom reactions, and the dashed line describes terrace facet scattering. (C) δ_{COM} computed on Pt(211) for all the trapped trajectories (blue) and for the trapped trajectories impacting first on the step (green) or on a terrace (red).

of time steps. Note that d_{xy} and d_{α} are dependent on the time step (0.4 fs) and on the total propagation time (i.e., the number of time steps T). On Pt(211), x and y are perpendicular and parallel to the step edge, respectively. If we consider d_{xy}, reported in Figure 5.6, it is noticeable how the molecules scattered from the step can travel significantly further than the ones scattered from the flat surface (Figures 5.6A and 5.6B). On average, we observe $\langle d_{xy} \rangle = 0.8$ Å on Pt(111) and $\langle d_{xy} \rangle = 2.8$ Å on Pt(211), but on the stepped surface, scattered molecules have been observed to travel up to 30 Å.

If we look at the trajectories trapped on the Pt(211) surface (Figure 5.6C), we can see that the molecules can travel considerable distances in our simulations (i.e., up to almost 50 Å) especially in the direction perpendicular to the step edge

(i.e., along x). Note that for these trajectories the propagation has been stopped after 2 ps and the longer we would propagate them the further they would travel. This is due to the large velocity the trapped molecules have in the xy plane. The distribution of the average velocity in xy upon trapping ($\langle v_{xy} \rangle^{trap}$) is reported in Figure 5.6D. $\langle v_{xy} \rangle^{trap}$ has been computed as:

$$\langle v_{xy} \rangle^{trap} = \sum_{t=1}^{N^{trap}} \frac{\sqrt{v_{x(t)}^2 + v_{y(t)}^2}}{N^{trap}}, \tag{5.7}$$

$\langle v_{xy} \rangle^{trap}$ is averaged over the total of N^{trap} time steps. Here t ranges from the first impact with the surface to the last step of the propagation (i.e., when the molecule is considered trapped). The velocity distribution is centered on $\langle v_{xy} \rangle^{trap} = 0.014$ Å/fs which means that during the estimated trapping time of 43 ps, those molecules can travel, on average, as far as 593 Å and this goes up to 642 Å if we consider only the molecules trapped after impinging on the step. This suggests that the trapped molecules have enough time to explore a large portion of the surface, increasing their chance of finding a favorable orientation to react or even a higher order defect with a lower dissociation barrier, such as kinks.

The importance of the energy transfer from motion normal to the surface to motion parallel to the surface can be quantified by calculating the amount of kinetic energy that molecules have in the xy plane after the impact with the surface (K_{xy}). To ensure a fair comparison, K_{xy} has been calculated at the end of the trajectory for scattered molecules and at the first outer turning point for trapped molecules. In Figure 5.7, K_{xy} is reported for scattered and trapped molecules on Pt(211) distinguishing between molecules which impact on the step facet and on the terrace facet. As expected, both trapped and scattered molecules show large values of K_{xy}. Moreover, the step site is more efficient than the terrace in promoting energy transfer to the parallel motion, probably because it makes a larger angle with the normal to the macroscopic surface.

In Figure 5.8, K_{xy} is reported as a function of the initial average collision en-

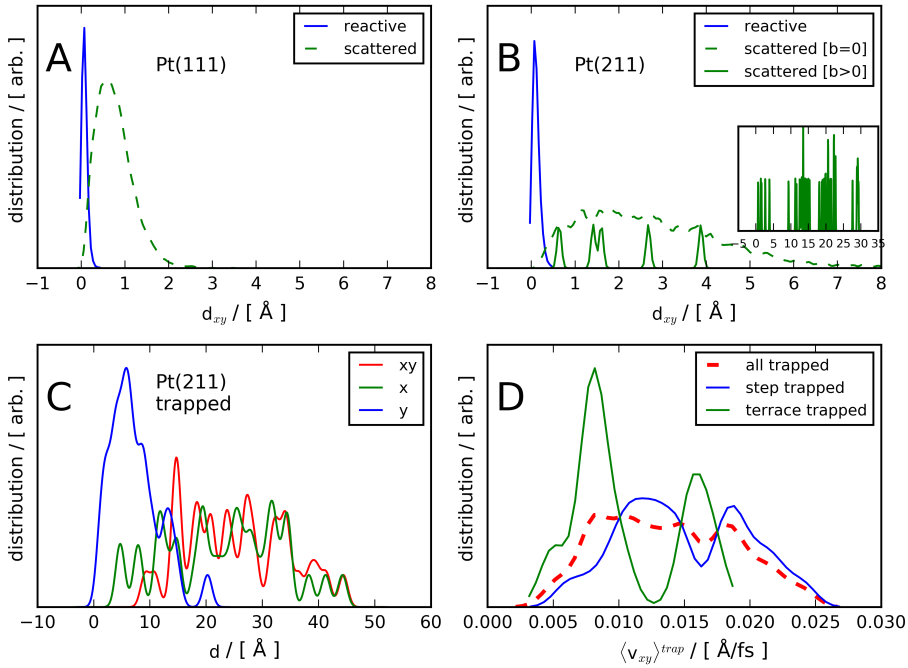

Figure 5.6: (A, B) distributions of the distance travelled by the molecules in the xy plane (d_{xy}) for reactive and scattered trajectories on the Pt(111) and Pt(211) surfaces, respectively. In panels A and B, the blue solid lines represent reactive trajectories (the distributions have been multiplied by 0.2 for a better comparison) and the green lines represent scattered trajectories without bouncing ($b = 0$, dashed green) and with bouncing ($b > 0$, solid green) on the surface. (C) distance travelled (d) by the molecules trapped on the Pt(211) surface. The distance travelled in the x direction, in the y direction, and the total distance travelled in the xy plane are reported in green, blue, and red, respectively. (D) distribution of average COM velocity in the xy plane for the trapped trajectories $\langle v_{xy} \rangle^{trap}$ for molecules that have the first impact on the terrace (green solid line), on the step (blue solid line), and for all the trapped molecules (red dashed line).

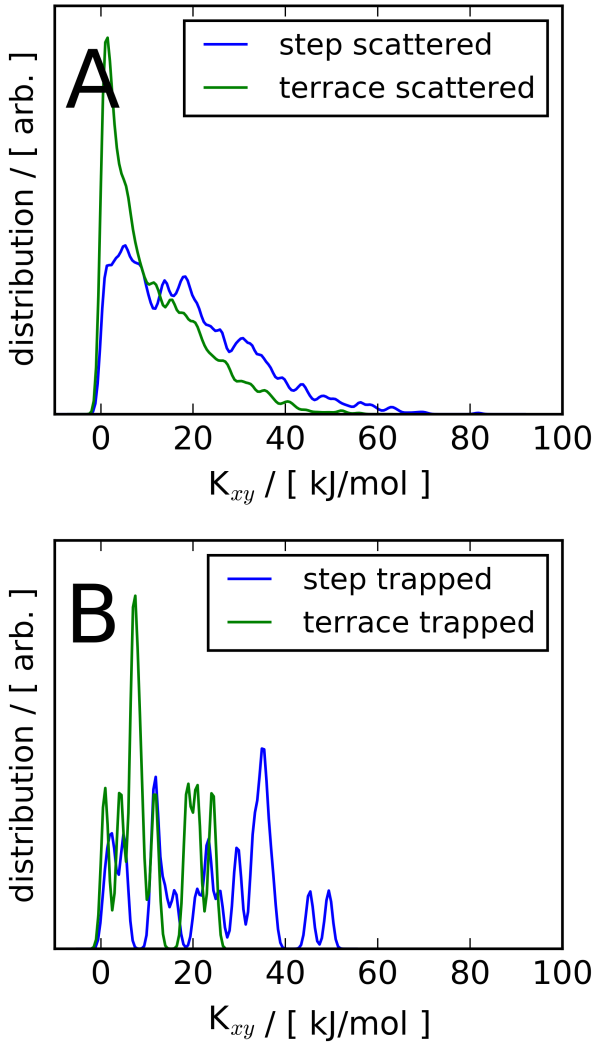

Figure 5.7: (A) distribution of kinetic energy in the xy plane (K_{xy}) after the impact with the Pt(211) surface for scattered molecules. (B) same of panel A but for trapped molecules. Results for molecules that impacted on the step and on the terrace are reported in blue and green, respectively.

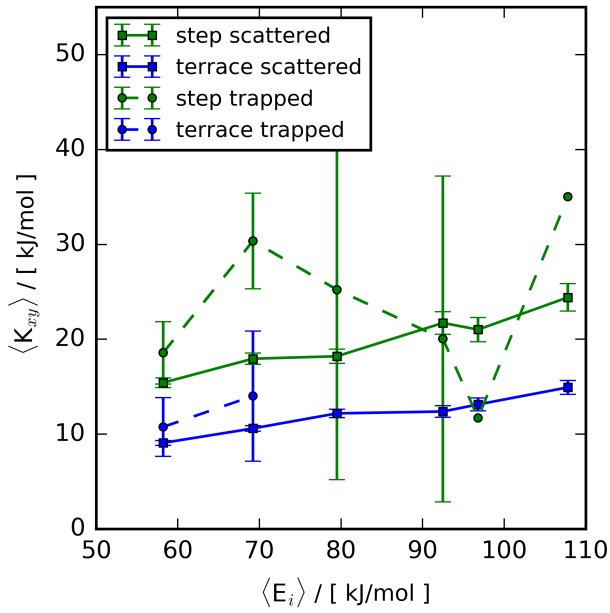

Figure 5.8: Average kinetic energy in the xy plane (K_{xy}) as a function of the average initial kinetic energy ($\langle E_i \rangle$) after the impact with the Pt(211) surface. Results for scattered molecules are reported as squares and solid lines and results for trapped molecules as circles and dashed lines. Green data represent molecules impacting on the step and blue data represent molecules impacting on the terrace. Two points are reported without error bars because the sample size for those data sets is 1. The lines are drawn to guide the eye.

ergy of the molecules ($\langle E_i \rangle$). The energy transfer to parallel translational motion increases with $\langle E_i \rangle$ and confirms that the step induces more energy transfer to the parallel motion than the terrace. The values of $\langle K_{xy} \rangle$ for the trapped trajectories show large error bars due to the small sample size, but the results suggest that the trapped molecules show a larger energy transfer to the parallel motion than the scattered ones at low $\langle E_i \rangle$ (Figure 5.8). In turn, this suggests that, especially at low $\langle E_i \rangle$, energy transfer to parallel motion at the step contributes to the trapping.

Out of a total of 34 trapped trajectories, 25 of them impacted on the step while only 9 on the terrace. If we weight these results according to the step:terrace area ratio (i.e., 1:1.8), we find that the trapping probability is 5 times larger if

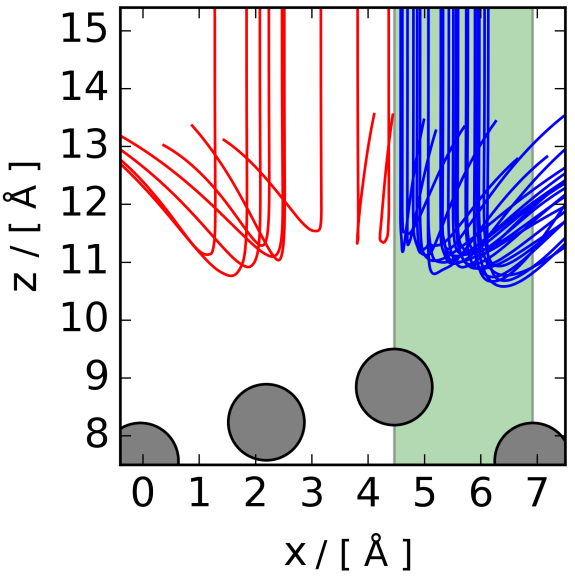

Figure 5.9: xz projection of the first part of the trapped trajectories. The first layer atoms 0 K positions are reported as gray circles and the step is highlighted in green. The trajectories are reported in blue if the first impact is on the step and in red if it is on the terrace.

the molecule impacts on the step than on the terrace. The xz projection of the first part of the trapped trajectories is reported in Figure 5.9. In Figure 5.10 the distribution of the average velocity in x for the trapped molecules ($\langle v_x \rangle^{trap}$) is reported. Again, these results suggest that one of the main reasons for the trapping we observe on Pt(211) is the geometry of the surface: the molecules that hit the step start travelling in the positive x direction. Most of the molecules impacting on the terrace travel in the negative x direction.

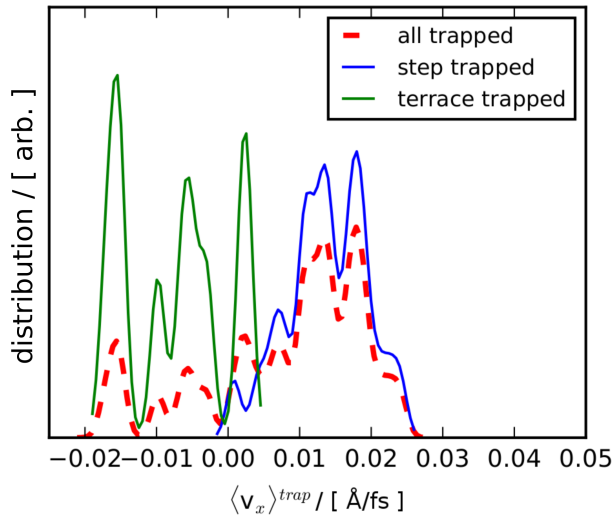

Figure 5.10: Distribution of the average velocity along x during trapping $\langle v_x \rangle^{trap}$ for all the trapped molecules (red line), the trapped molecules that have the first impact on the step (blue line), and the ones that have the first impact on the terrace (green line).

5.3.3 Energy Transfer to Surface Phonons

The energy transfer from the molecules to the surface phonons (E_T) is reported in Figure 5.11. All the scattered molecules transfer roughly the same amount of energy to the phonons independently from the Pt surface on which they impact; on average, molecules that hit the Pt(111) and the Pt(211) surface show $\langle E_T \rangle = 15.5 \pm 0.2$ and 13.9 ± 0.2 kJ/mol, respectively. Note that Pt(111) shows a somewhat larger $\langle E_T \rangle$, but the AIMD trajectories have been performed over a larger range of $\langle E_i \rangle$. This can be seen in Figure 5.11B where E_T is reported as a function of the incident energy: the linear regression for the two sets of data shows the same slope (i.e., 0.165) and very similar intercepts (i.e., 0.914 kJ/mol and 1.400 kJ/mol for Pt(111) and Pt(211), respectively). Note that the difference of 0.486 kJ/mol in the intercept is smaller than the average error for both surfaces (i.e., 0.527 kJ/mol and 0.514 kJ/mol for Pt(111) and Pt(211), respectively). The small number of trapped trajectories reduces the statistical significance of their analysis. However the results suggest that, especially at

low $\langle E_i \rangle$, some trajectories can undergo a larger energy transfer to the surface phonons (i.e., $\langle E_T \rangle = 23.2 \pm 1.9$ kJ/mol) which would increase the probability of being trapped. This suggests that energy transfer to the phonons contributes to the trapping on Pt(211).

The E_T has been calculated approximately from the molecular kinetic (K) and potential (V) energy. The initial configuration (i) is always the first step of the dynamics. For the scattered molecule, the final configuration (f) is taken from the last step of the dynamics, while for the trapped molecule, we considered the E_T upon first impact with the surface, and therefore, the final configuration is taken from the first outer turning point configuration. This means that, in the initial and in the final configurations, the molecules might not be at the same distance from the slab. Therefore the energy transfer has been estimated using Equation 5.8, which includes a correction for the interaction energy (I). I has been computed using Equation 5.9 and subtracting the absolute energy of the isolated CHD_3 and of the bare slab from the energy of the system containing both the molecule and the metal surface:

$$E_T = -\big[\big(K_f + V_f + I_f\big) - \big(K_i + V_i + I_i\big)\big], \tag{5.8}$$

$$I = V_{slab+CHD_3} - V_{slab} - V_{CHD_3}. \tag{5.9}$$

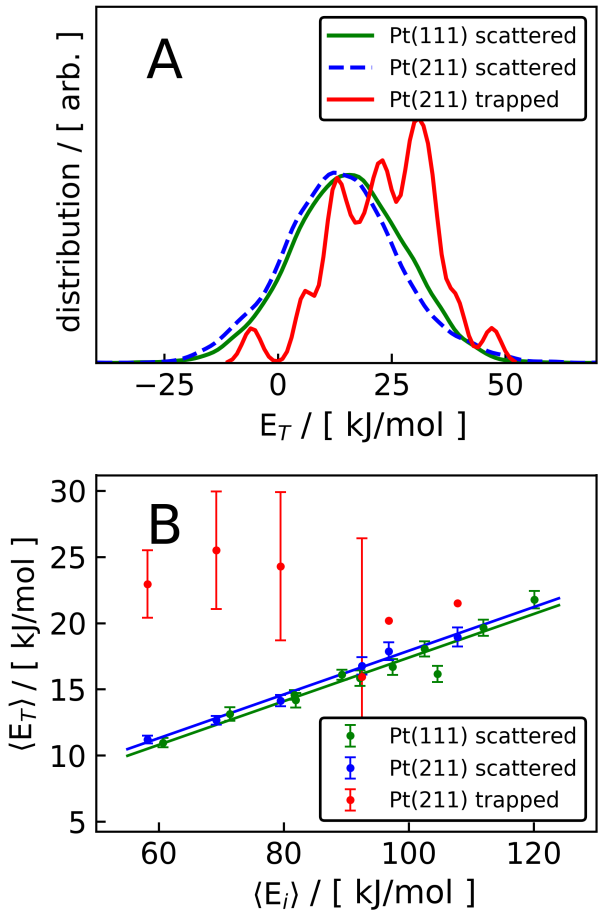

Figure 5.11: (A) energy transfer to the surface (E_T). Results are reported for scattered molecules on the flat Pt(111) (green line), on the stepped Pt(211) (blue line), and for trapped molecules (after the first impact on the Pt(211)) (red line). (B) average energy transfer to the surface versus average incident energy ($\langle E_i \rangle$). Results are reported for scattered molecules on the flat Pt(111) (green), on the stepped Pt(211) (blue), and for trapped molecules (after the first impact on the Pt(211)) (red). The lines are linear regressions of the data. Note that error bars are not shown for samples containing only one trapped trajectory.

5.3.4 Reaction Site and Dissociation Geometry

On Pt(211), the vast majority of the reactive events happen on the step edge. The reaction site has been studied by measuring the distance in the xy plane from the center of mass of the molecule to the closest atom in the first layer and reporting the distributions for all the trajectories simulated. The results are reported in Figure 5.12A for Pt(111) and in Figure 5.12B for Pt(211) for the reacted molecules at $t = 0$ and at the time of the dissociation ($t = t_{diss}$). For both surfaces, the reaction happens preferentially close to top sites (i.e., atoms in the first layer), but for the stepped surface, a considerable number of molecules dissociate further than 1 Å away from the closest Pt atom.

The effect of the orientation of the molecules on the reaction has been analyzed by monitoring the β (Figure 5.13), the θ (Figure 5.14), and the γ (Figure 5.15) angles throughout the dynamics and investigating their dependence on $\langle E_i \rangle$ (Figure 5.16). These three angles describe the orientation of the umbrella axis (β) and of the dissociating bond (θ) with respect to the surface normal and the angle between the dissociating bond and the umbrella axis (γ) (see Figure 5.3). The angles have been computed at the start of the trajectories ($t = 0$) and at the time of the dissociation ($t = t_{diss}$) for the reactive trajectories. For both θ and β, the initial distribution considering all the molecules simulated is a sine distribution proving the accurate random sampling of the initial conditions.

Comparing the Pt(111) results to the Pt(211) results, one can see that the dissociation dynamics on the two surfaces are qualitatively very similar: the two known key aspects of the dissociation of CHD_3 on Pt and Ni are the pre-orientation of the dissociating bond [4, 5] and the umbrella reorientation [4]. The distributions of θ reported in Figure 5.14 show that only bonds initially pointing toward the surface (i.e., close to the TS value of $\theta \approx 133°$) can dissociate and that the angular acceptance range for the dissociation on the Pt(211) surface is broader as the final θ distributions are less localized and exhibit larger σ values (see Figure 5.14 and Table 5.2).

The results for β (see Figure 5.13) confirm the important role of the umbrella

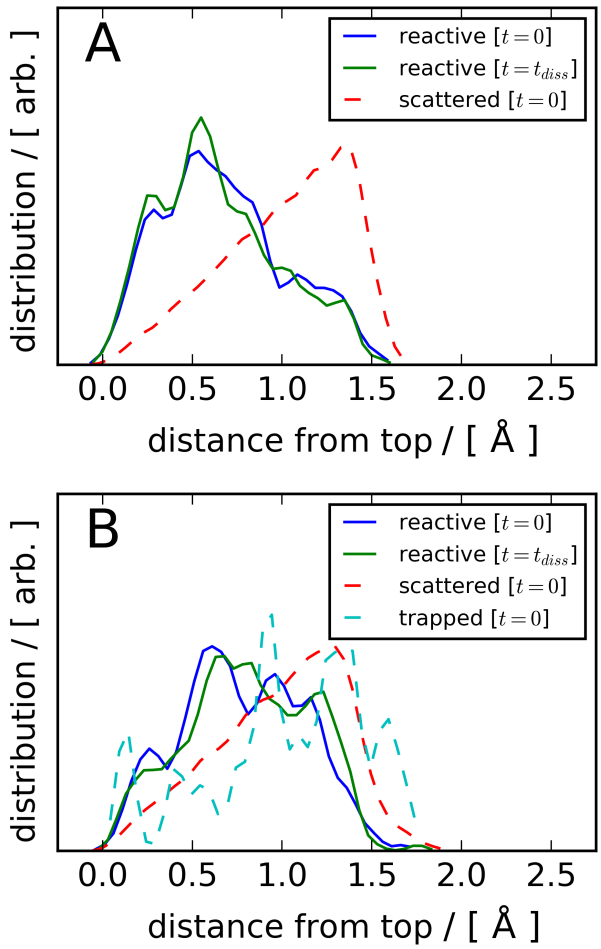

Figure 5.12: Distance from the closest top site in xy. (A, B) results for the Pt(111) surface and for the Pt(211) surface, respectively. Results for reactive trajectories are reported in blue and green for the initial position and the position at the dissociation time, respectively. Results for scattered and trapped trajectories are reported in red and cyan, respectively.

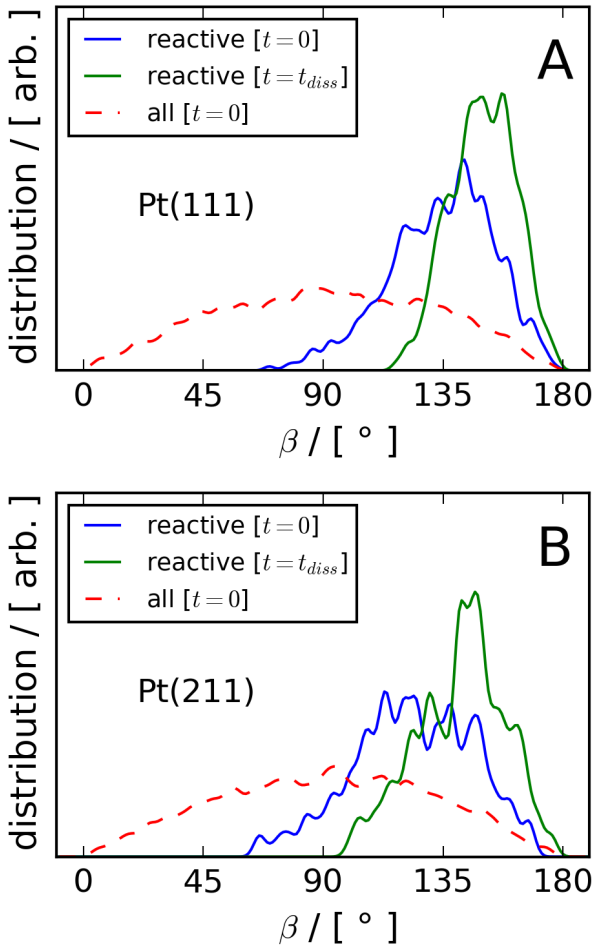

Figure 5.13: (A) β distributions for CHD_3 on Pt(111). Results for the reactive trajectories are reported in blue and green for the initial and the dissociation step, respectively. Results for the first time step of all the trajectories are reported in red. (B) the same as panel A but for Pt(211).

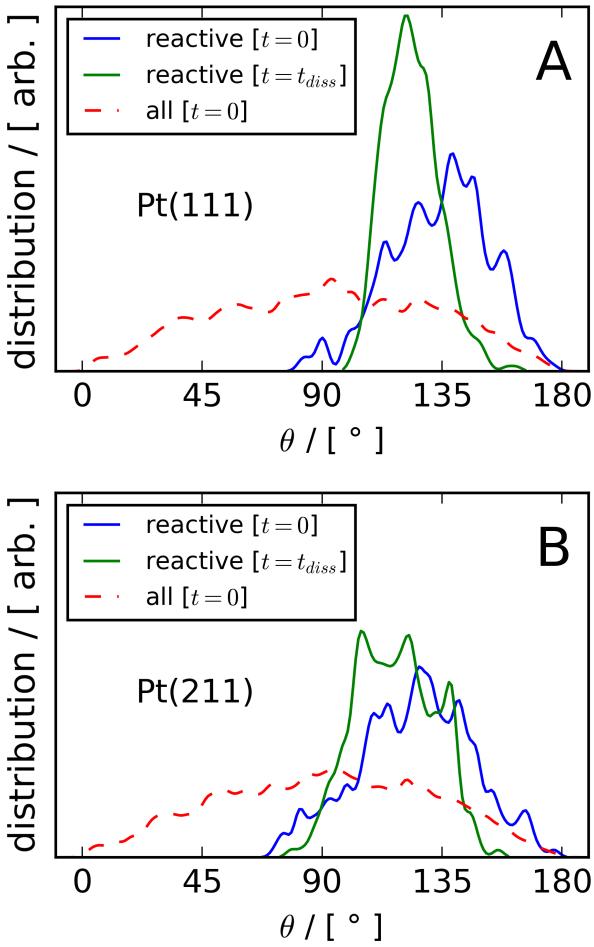

Figure 5.14: The same as Figure 5.13 but for θ.

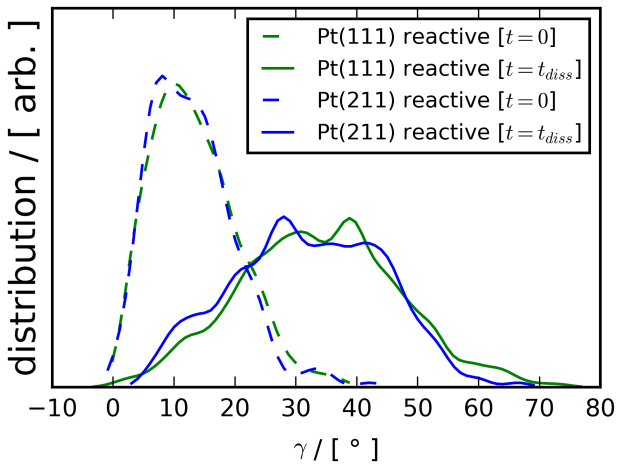

Figure 5.15: γ distributions for $t = 0$ and for the dissociation step as dashed and solid lines, respectively. Green lines are for Pt(111) results, and blue lines are for Pt(211) results.

	β / [∘]		θ / [∘]		γ [∘]	
Surface	$\langle\beta\rangle \pm \sigma_M$	σ	$\langle\theta\rangle \pm \sigma_M$	σ	$\langle\gamma\rangle \pm \sigma_M$	σ
Pt(111)	149.9 ± 0.6	12.1	123.6 ± 0.5	10.2	33.8 ± 0.6	13.0
Pt(211)	141.2 ± 1.1	16.7	117.3 ± 1.0	15.0	31.9 ± 0.8	12.2

Table 5.2: Average value, standard deviation (σ), and standard error (σ_M) for β, θ, and γ at the time of the dissociation as reported in Figures 5.13, 5.14 and 5.15, respectively.

reorientation [4] for CHD_3 on Pt(111) and extend this confirmation to the reaction on the stepped Pt(211) surface as well. In order to react, the molecule not only needs to approach the surface with the CH bond pre-oriented toward the surface, but in the meantime the umbrella has to swing upwards increasing the value of β. In previous work [4] , Füchsel *et al.* studied the dissociation of CHD_3 on Pt(111) and, for $\langle E_i \rangle$ between 49 and 84 kJ/mol, they observed that the centers of the distributions of θ do not shift during the reaction. Extending the range of initial average kinetic energy, we do observe a dependence of θ and of γ on $\langle E_i \rangle$ at the time of the reaction (see Figure 5.16) that can be explained by considering that, since the hydrogen (or deuterium) atom is oriented toward the surface,

the dissociating bond bends away from the surface upon impacting on the slab proportionally to the COM velocity, and this results in a decrease of θ and in an increase of γ (since β does not depend on $\langle E_i \rangle$).

Figure 5.16 also shows that, at the moment of the dissociation, β and θ (Figures 5.16A and 5.16B) are smaller for Pt(211) than for Pt(111), while γ is very similar (Figure 5.16C). This suggests that at the moment of the reaction the internal molecular geometry is the same on the two surfaces. However the molecules react, on average, more parallel to the macroscopic surface for the stepped Pt(211). This can be explained by looking at the θ angle of the TSs on the two surfaces. All the TSs on Pt(111) show $\theta \approx 133°$ (see Table III in Ref. [49]) which is the same value of the lowest E_b TS on Pt(211) (Edge2Edge-B1 in Figure 5.4 and Table 5.1). However, the TSs perpendicular to the step edge on Pt(211) (i.e., C, D, and E in Table 5.1) show values of θ about 10°–19° smaller and this effectively broadens the angular acceptance range for the dissociation on the stepped surface. The TSs C, D, and E dissociate in the direction perpendicular to the step edge and, even though they show larger E_b, they play a big role in the dissociative process. In Figure 5.17, the distribution of the angle α is plotted at $t = 0$ and the moment of the dissociation for molecules reacting on the step edge atom. α is defined as the counter-clockwise angle between x and the projection of the dissociating bond on the xy plane. Therefore, $\alpha = 0°$ corresponds to a dissociation in the x direction and $\alpha = 90°$ corresponds to the y direction (i.e., perpendicular and parallel to the step edge, respectively). Even though the minimum energy barrier TS occurs at $\alpha \approx 90°$ (and, equivalently, at $\alpha \approx 270°$), most of the reactions on the step edge atom happen for $\alpha \approx 180°$. This can be partially explained taking into account that the orientation of the molecules is sampled as $\sin(\theta)$ which makes $\theta \approx 114°$ (i.e., the ideal value for $\alpha = 180°$) oversampled with respect to $\theta \approx 133°$ (i.e., the ideal value for $\alpha = 90°$) (see Table 5.1).

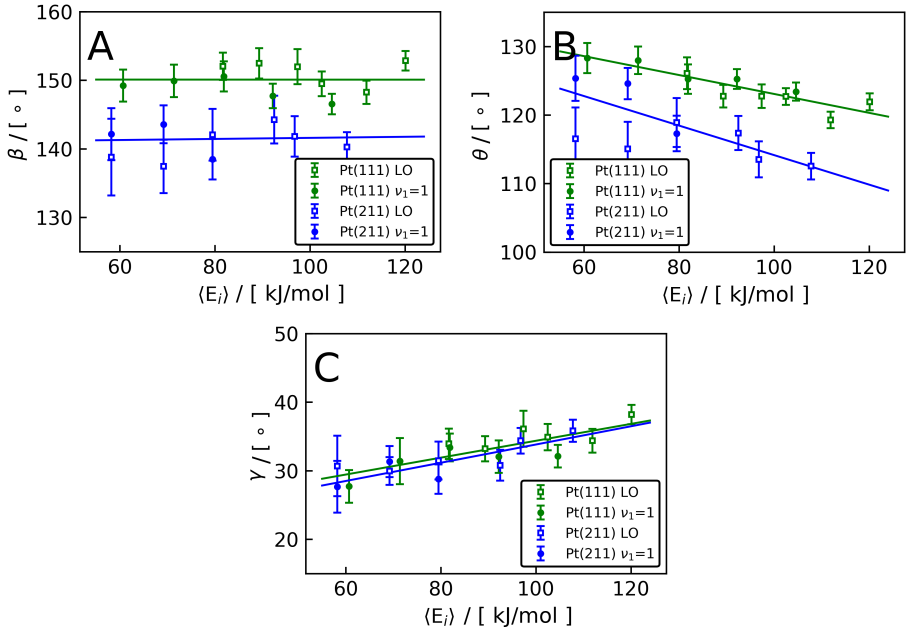

Figure 5.16: Dependence of β, θ and γ on $\langle E_i \rangle$ the moment of the dissociation. Results for the Pt(111) and for the Pt(211) are reported in green and blue, respectively. Open squares represent laser-off (LO) calculations, and filled circles represent $\nu_1 = 1$ calculations. The linear regressions reported are computed considering both LO and $\nu_1 = 1$ trajectories.

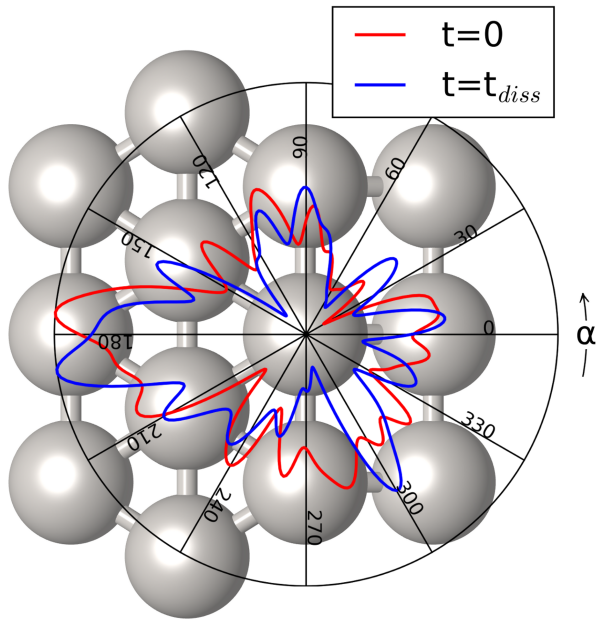

Figure 5.17: Distribution of α at $t = 0$ and at the time of the dissociation (t_{diss}) (in red and blue, respectively) for molecules that reacted on the step edge atom. The value of α is reported in black and it increases counter-clockwise. The plot is superimposed on the Pt(211) 1^{st} layer top view. The closer the distribution is to the external black circle, the more the value of α is represented.

5.4 Summary and Conclusions

In this Chapter, we have analyzed a total of 12500 trajectories where CHD_3 is impinging either on the flat Pt(111) or on the stepped Pt(211) surface. Moreover several different TSs have been found on the Pt(211) surface. The TSs found all have a very similar molecular geometry and the ones located on a step edge atom of the Pt(211) surface show a significantly lower energy barrier. The ones on the terrace middle atom have larger barrier heights, even larger than for the flat Pt(111) surface. On both surfaces, the dissociation has been shown to proceed through a very similar mechanism where the dissociative CH bond needs to be pre-oriented toward the surface and the methyl umbrella rotates upwards to promote the reaction. However the stepped Pt(211) has a broader angular acceptance range for the dissociative chemisorption and the molecules react on average more parallel to the surface. The stepped Pt(211) surface can trap molecules due to a larger energy transfer to phonons and to corrugation-promoted energy transfer to parallel translational motion. The large velocity in the direction parallel to the surface of the trapped trajectories suggests that they can travel long distances, on average more than 600 Å for step impacts with trapping times > 1 ps, while bouncing on the surface. This implies that, in experiments, the trapped molecule has time to explore the surface, and therefore, it has an increased probability of reacting by finding the most favorable geometry or even a higher order defect, such as a kink.

Bibliography

[1] C. A. Wolcott, A. J. Medford, F. Studt, and C. T. Campbell, "Degree of Rate Control Approach to Computational Catalyst Screening," *J. Catal.*, vol. 330, pp. 197–207, 2015.

[2] Y. Xu, A. C. Lausche, S. G. Wang, T. S. Khan, F. Abild-Pedersen, F. Studt, J. K. Nørskov, and T. Bligaard, "In Silico Search for Novel Methane Steam Reforming Catalysts," *New J. Phys.*, vol. 15, p. 125021, 2013.

[3] D. Migliorini, H. Chadwick, F. Nattino, A. Gutiérrez-González, E. Dombrowski, E. A. High, H. Guo, A. L. Utz, B. Jackson, R. D. Beck, and G. J. Kroes, "Surface Reaction Barriometry: Methane Dissociation on Flat and Stepped Transition-Metal Surfaces," *J. Phys. Chem. Lett.*, vol. 8, pp. 4177–4182, 2017.

[4] G. Füchsel, P. S. Thomas, J. den Uyl, Y. Öztürk, F. Nattino, H. D. Meyer, and G. J. Kroes, "Rotational Effects on the Dissociation Dynamics of CHD_3 on Pt(111)," *Phys. Chem. Chem. Phys.*, vol. 18, pp. 8174–8185, 2016.

[5] F. Nattino, D. Migliorini, G. J. Kroes, E. Dombrowski, E. A. High, D. R. Killelea, and A. L. Utz, "Chemically Accurate Simulation of a Polyatomic Molecule-Metal Surface Reaction," *J. Phys. Chem. Lett.*, vol. 7, pp. 2402–2406, 2016.

[6] F. Nattino, D. Migliorini, M. Bonfanti, and G. J. Kroes, "Methane Dissociation on Pt(111): Searching for a Specific Reaction Parameter Density Functional," *J. Chem. Phys.*, vol. 144, p. 044702, 2016.

[7] H. Guo and B. Jackson, "Mode- and Bond-Selective Chemistry on Metal Surfaces: The Dissociative Chemisorption of CHD_3 on Ni(111)," *J. Phys. Chem. C*, vol. 119, pp. 14769–14779, 2015.

[8] S. Nave and B. Jackson, "Methane Dissociation on Ni(111): The Role of Lattice Reconstruction," *Phys. Rev. Lett.*, vol. 98, p. 173003, 2007.

[9] A. K. Tiwari, S. Nave, and B. Jackson, "The Temperature Dependence of Methane Dissociation on Ni(111) and Pt(111): Mixed Quantum-Classical Studies of the Lattice Response," *J. Chem. Phys.*, vol. 132, p. 134702, 2010.

[10] X. J. Shen, Z. J. Zhang, and D. H. Zhang, "Communication: Methane Dissociation on Ni(111) Surface: Importance of Azimuth and Surface Impact Site," *J. Chem. Phys.*, vol. 144, p. 101101, 2016.

[11] R. R. Smith, D. R. Killelea, D. F. DelSesto, and A. L. Utz, "Preference for Vibrational over Translational Energy in a Gas-Surface Reaction," *Science*, vol. 304, pp. 992–995, 2004.

[12] D. R. Killelea, V. L. Campbell, N. S. Shuman, and A. L. Utz, "Bond-Selective Control of a Heterogeneously Catalyzed Reaction," *Science*, vol. 319, pp. 790–793, 2008.

[13] R. D. Beck, P. Maroni, D. C. Papageorgopoulos, T. T. Dang, M. P. Schmid, and T. R. Rizzo, "Vibrational Mode-Specific Reaction of Methane on a Nickel Surface," *Science*, vol. 302, pp. 98–100, 2003.

[14] B. L. Yoder, R. Bisson, and R. D. Beck, "Steric Effects in the Chemisorption of Vibrationally Excited Methane on Ni(100)," *Science*, vol. 329, pp. 553–556, 2010.

[15] J. M. Wei and E. Iglesia, "Mechanism and Site Requirements for Activation and Chemical Conversion of Methane on Supported Pt Clusters and Turnover Rate Comparisons among Noble Metals," *J. Phys. Chem. B*, vol. 108, pp. 4094–4103, 2004.

[16] B. Jiang, R. Liu, J. Li, D. Q. Xie, M. H. Yang, and H. Guo, "Mode Selectivity in Methane Dissociative Chemisorption on Ni(111)," *Chem. Sci.*, vol. 4, pp. 3249–3254, 2013.

[17] X. J. Shen, J. Chen, Z. J. Zhang, K. J. Shao, and D. H. Zhang, "Methane Dissociation on Ni(111): A Fifteen-Dimensional Potential Energy Surface Using Neural Network Method," *J. Chem. Phys.*, vol. 143, p. 144701, 2015.

[18] P. M. Hundt, B. Jiang, M. E. van Reijzen, H. Guo, and R. D. Beck, "Vibrationally Promoted Dissociation of Water on Ni(111)," *Science*, vol. 344, pp. 504–507, 2014.

[19] S. Nave and B. Jackson, "Vibrational Mode-Selective Chemistry: Methane Dissociation on Ni(100)," *Phys. Rev. B*, vol. 81, p. 233408, 2010.

[20] B. Jackson and S. Nave, "The Dissociative Chemisorption of Methane on Ni(111): The Effects of Molecular Vibration and Lattice Motion," *J. Chem. Phys.*, vol. 138, p. 174705, 2013.

[21] A. Farjamnia and B. Jackson, "The Dissociative Chemisorption of Water on Ni(111): Mode- and Bond-Selective Chemistry on Metal Surfaces," *J. Chem. Phys.*, vol. 142, p. 234705, 2015.

[22] G. J. Kroes, "Toward a Database of Chemically Accurate Barrier Heights for Reactions of Molecules with Metal Surfaces," *J. Phys. Chem. Lett.*, vol. 6, pp. 4106–4114, 2015.

[23] C. Díaz, E. Pijper, R. A. Olsen, H. F. Busnengo, D. J. Auerbach, and G. J. Kroes, "Chemically Accurate Simulation of a Prototypical Surface Reaction: H_2 Dissociation on Cu(111)," *Science*, vol. 326, pp. 832–834, 2009.

[24] L. Sementa, M. Wijzenbroek, B. J. van Kolck, M. F. Somers, A. Al-Halabi, H. F. Busnengo, R. A. Olsen, G. J. Kroes, M. Rutkowski, C. Thewes, N. F. Kleimeier, and H. Zacharias, "Reactive Scattering of H_2 from Cu(100): Comparison of Dynamics Calculations Based on the Specific Reaction Parameter Approach to Density Functional Theory with Experiment," *J. Chem. Phys.*, vol. 138, p. 044708, 2013.

[25] E. Nour Ghassemi, M. Wijzenbroek, M. F. Somers, and G. J. Kroes, "Chemically Accurate Simulation of Dissociative Chemisorption of D_2 on Pt(111)," *J. Chem. Phys. Lett.*, vol. 683, pp. 329–335, 2017.

[26] Y. Y. Chuang, M. L. Radhakrishnan, P. L. Fast, C. J. Cramer, and D. G. Truhlar, "Direct Dynamics for Free Radical Kinetics in Solution: Solvent

Effect on the Rate Constant for the Reaction of Methanol with Atomic Hydrogen," *J. Phys. Chem. A*, vol. 103, pp. 4893–4909, 1999.

[27] B. Hammer, L. B. Hansen, and J. K. Nørskov, "Improved Adsorption Energetics Within Density-Functional Theory Using Rrevised Perdew-Burke-Ernzerhof Functionals," *Phys. Rev. B*, vol. 59, pp. 7413–7421, 1999.

[28] J. P. Perdew, K. Burke, and M. Ernzerhof, "Generalized Gradient Approximation Made Simple," *Phys. Rev. Lett.*, vol. 77, pp. 3865–3868, 1996.

[29] J. P. Perdew, K. Burke, and M. Ernzerhof, "Erratum: Generalized Gradient Approximation Made Simple," *Phys. Rev. Lett.*, vol. 78, p. 1396, 1997.

[30] G. Román-Pérez and J. M. Soler, "Efficient Implementation of a van der Waals Density Functional: Application to Double-Wall Carbon Nanotubes," *Phys. Rev. Lett.*, vol. 103, p. 096102, 2009.

[31] M. Dion, H. Rydberg, E. Schröder, D. C. Langreth, and B. I. Lundqvist, "Van der Waals Density Functional for General Geometries," *Phys. Rev. Lett.*, vol. 92, p. 246401, 2004.

[32] H. S. Taylor, "A Theory of the Catalytic Surface," *Proc. R. Soc. Lond. A*, vol. 108, pp. 105–111, 1925.

[33] T. Zambelli, J. Wintterlin, J. Trost, and G. Ertl, "Identification of the "Active Sites" of a Surface-Catalyzed Reaction," *Science*, vol. 273, pp. 1688–1690, 1996.

[34] B. Hammer, "Bond Activation at Monatomic Steps: NO Dissociation at Corrugated Ru(0001)," *Phys. Rev. Lett.*, vol. 83, pp. 3681–3684, 1999.

[35] A. T. Gee, B. E. Hayden, C. Mormiche, A. W. Kleyn, and B. Riedmüller, "The Dynamics of the Dissociative Adsorption of Methane on Pt(533)," *J. Chem. Phys.*, vol. 118, pp. 3334–3341, 2003.

[36] F. Abild-Pedersen, O. Lytken, J. Engbæk, G. Nielsen, I. Chorkendorff, and J. K. Nørskov, "Methane Activation on Ni(111): Effects of Poisons and Step Defects," *Surf. Sci.*, vol. 590, pp. 127–137, 2005.

[37] G. Kresse and J. Hafner, "Ab Initio Molecular-Dynamics Simulation of the Liquid-Metal-Amorphous-Semiconductor Transition in Germanium," *Phys. Rev. B*, vol. 49, pp. 14251–14269, 1994.

[38] G. Kresse and J. Furthmüller, "Efficient Iterative Schemes for Ab Initio Total-Energy Calculations Using a Plane-Wave Basis Set," *Phys. Rev. B*, vol. 54, pp. 11169–11186, 1996.

[39] G. Kresse and J. Furthmüller, "Efficiency of Ab-Initio Total Energy Calculations for Metals and Semiconductors Using a Plane-Wave Basis Set," *Comput. Mater. Sci*, vol. 6, pp. 15–50, 1996.

[40] G. Kresse and J. Hafner, "Ab Initio Molecular Dynamics for Liquid Metals," *Phys. Rev. B*, vol. 47, pp. 558–561, 1993.

[41] P. E. Blöchl, "Projector Augmented Wave-Method," *Phys. Rev. B*, vol. 50, pp. 17953–17979, 1994.

[42] G. Kresse and D. Joubert, "From Ultrasoft Pseudopotentials to the Projector Augmented-Wave Method," *Phys. Rev. B*, vol. 59, pp. 1758–1775, 1999.

[43] H. Chadwick, A. Gutiérrez-González, and R. D. Beck, "Quantum State Resolved Molecular Beam Reflectivity Measurements: CH_4 Dissociation on Pt(111)," *J. Chem. Phys.*, vol. 145, p. 174707, 2016.

[44] P. H. Xiao, D. Sheppard, J. Rogal, and G. Henkelman, "Solid-State Dimer Method for Calculating Solid-Solid Phase Transitions," *J. Chem. Phys.*, vol. 140, p. 174104, 2014.

[45] J. Kästner and P. Sherwood, "Superlinearly Converging Dimer Method for Transition State Search," *J. Chem. Phys.*, vol. 128, p. 014106, 2008.

[46] A. Heyden, A. T. Bell, and F. J. Keil, "Efficient Methods for Finding Transition States in Chemical Reactions: Comparison of Improved Dimer Method and Partitioned Rational Function Optimization Method," *J. Chem. Phys.*, vol. 123, p. 224101, 2005.

[47] G. Henkelman and H. Jónsson, "A Dimer Method for Finding Saddle Points on High Dimensional Potential Surfaces Using Only First Derivatives," *J. Chem. Phys.*, vol. 111, pp. 7010–7022, 1999.

[48] D. Migliorini, H. Chadwick, and G. J. Kroes, "Methane on a Stepped Surface: Dynamical Insights on the Dissociation of CHD_3 on Pt(111) and Pt(211)," *J. Chem. Phys.*, vol. 149, p. 094701, 2018.

[49] S. Nave, A. K. Tiwari, and B. Jackson, "Methane Dissociation and Adsorption on Ni(111), Pt(111), Ni(100), Pt(100), and Pt(110)-(1×2): Energetic Study," *J. Chem. Phys.*, vol. 132, p. 054705, 2010.